Received: 3 March 2020 | Revised: 11 July 2020 | Accepted: 12 July 2020

DOI: 10.1002/jrs.5955

RESEARCH ARTICLE

Journal of RAMAN SPECTROSCOPY WILEY

Toward standardization of Raman spectroscopy: Accurate wavenumber and intensity calibration using rotational Raman spectra of H_2, HD, D_2, and vibration–rotation spectrum of O_2

Ankit Raj[1] | **Chihiro Kato**[2] | **Henryk A. Witek**[1,3] | **Hiro-o Hamaguchi**[1,3]

[1]Department of Applied Chemistry and Institute of Molecular Science, National Chiao Tung University, Hsinchu, Taiwan

[2]Department of Chemical Engineering, Kanagawa Institute of Industrial Science and Technology (KISTEC), Ebina, Kanagawa, Japan

[3]Center for Emergent Functional Matter Science, National Chiao Tung University, Hsinchu, Taiwan

Correspondence
Henryk A. Witek and Hiro-o Hamaguchi, Department of Applied Chemistry and Institute of Molecular Science, National Chiao Tung University, Hsinchu 30010, Taiwan.
Email: hwitek@mail.nctu.edu.tw; hhama@nctu.edu.tw

Funding information
Ministry of Science and Technology, Taiwan, Grant/Award Numbers: MOST103-2113- M-009-001, MOST105-2923-M-009-001-MY3, MOST108-2113-M-009-010-MY3; Center for Emergent Functional Matter Science of National Chiao Tung University

Abstract

Wavenumber and intensity calibration of a Raman spectrometer is performed with the use of pure rotational Raman bands ($\Delta\nu = 0, \Delta J = \pm 2$) of H_2, HD, D_2, and vibration–rotation Raman bands ($\Delta\nu = 1, \Delta J = \pm 2$) of O_2 as primary standards. Wavenumber calibration is based on reference transition wavenumbers available from accurate theoretical and experimental results. Intensity calibration is based on ratios of accurate theoretical Raman intensities for transitions from common rotational states to eliminate temperature effects. Polarization dependence is corrected to ensure that all of these bands have the correct depolarization ratio, $\rho = 0.75$. The calibrated Raman spectrometer is used to measure standard Raman spectra of carbon tetrachloride, benzene, cyclohexane, toluene, and benzonitrile, for which the relative Raman intensities and depolarization ratios are determined with carefully estimated uncertainties. Vibrational frequencies of indene used for routine wavenumber calibration are updated.

KEYWORDS

depolarization ratio, intensity calibration, quantitative Raman spectroscopy, standard Raman spectra, wavenumber calibration

1 | INTRODUCTION

Modern Raman spectroscopy, together with infrared (IR) spectroscopy, constitutes the two major techniques of vibrational spectroscopy used in many fields. However, wavenumber and intensity accuracies of measurements performed with contemporary Raman spectrometers are inferior to those performed with present IR spectrometers. Wavenumber accuracy of Fourier transform infrared spectroscopy (FT-IR) is guaranteed by highly accurate interferometric calibration of the interferogram with the use of a laser. IR intensities in the form of absorbance are free from instrumental bias because absorbance is obtained from the intensity ratio I/I_0, where I and I_0 are the IR intensities with and without sample, measured under the same instrumental conditions. As a result, standardization of IR spectroscopy is well advanced with an accumulation of numerous standard IR spectra available in the form of data banks. Raman spectroscopy is less developed instrumentally in this respect; it urgently needs standardization with better wavenumber and intensity accuracies, which can be achieved via accurate calibration of spectrometers.

Accurate calibration of Raman spectrometers is also a requisite for quantitative Raman spectroscopy, by which we can determine the absolute concentrations of molecules. The absolute quantitativeness is a shortcoming of IR spectroscopy, which requires accurate path length determination for converting intensities to concentrations. Determination of absolute concentrations from Raman spectra requires the knowledge of absolute Raman cross-sections, which plays an important role in the process of standardization of Raman spectroscopy. Employing a reference with known absolute Raman cross-section, Raman cross-sections are obtainable by relative intensity measurements, if and only if an accurately calibrated Raman spectrometer is used.

Calibration of Raman spectrometers has been the subject of several past reviews and books.[1–5] For wavenumber calibration, atomic emission lines from neon[6,7] and Ar^+/Kr^+ ions[8] are used as absolute primary standards. These absolute standards require the knowledge of accurate laser wavelength so as to convert absolute wavenumbers to relative wavenumbers (or Raman shift); for example, an uncertainty of $\pm$0.005 nm in the laser wavelength introduces an error of 0.18 cm^{-1} in the corresponding relative wavenumbers, at 532 nm. Raman bands of solvents like indene, cyclohexane, and toluene are also used as wavenumber standards.[3,9] Although these wavenumber standards are conveniently used in many practical applications, the applicable spectral range is limited. Also, the calibration accuracy is restricted by the uncertainty in the band fitting analysis. For intensity calibration, black-body emission from a tungsten lamp is used.[10,11] Black-body emission is a primary intensity standard because its spectrum can be calculated to a high accuracy without employing approximations. However, its spectrum tends to fluctuate due to its high sensitivity to temperature and current.[12] The emission spectrum also changes significantly depending on the position of the lamp relative to the slit of the spectrometer, and hence, the experimental setup requires a precise placement of the lamp exactly at the sample position.[13–15] Emission spectra from molecules like quinine, coumarin 540a, Kopp 2412 glass, and so forth are also used as luminescence standards.[15–17] Luminescence standards need excitation sources, which may be different from the laser used for Raman excitation. Luminescence standards bear relatively large error of 5%–10%, and for this reason, they seem less attractive for the present purpose of accurate intensity calibration of Raman spectrometer.

Intensity calibration using Raman intensities was first demonstrated by Hamaguchi et al.,[18] who used the rotational Raman intensities from D_2 with five different excitation lines from an argon ion laser, for calibration in the wavelength region 455–529 nm. Montero et al.[13] used anti-Stokes to Stokes intensity ratios from H_2 with five lines from an argon ion laser at room temperature to calibrate a similar spectral region. Okajima and Hamaguchi[19] demonstrated accurate intensity calibration of the low wavenumber region spanning −150 to 150 cm^{-1} Raman shift using pairs of pure rotational Raman bands of N_2 originating from common rotational states. Schlösser et al.[20] used the Q-branches of H_2, HD, D_2, HT, DT, and T_2 to calibrate the high wavenumber region 2,490–4,170 cm^{-1}. In these approaches, the observed intensities or intensity ratios are compared with theoretical values as references. Least squares fitting of the observed values to the theoretical data yields a wavelength-dependent sensitivity curve for intensity calibration.

In the present work, we undertake further steps toward accurate wavenumber and intensity calibration of Raman spectrometers using the pure rotational Raman bands of H_2, HD, and D_2 and the vibration–rotation bands of O_2. For wavenumber calibration, theoretical and experimental wavenumbers accurately determined for H_2 and D_2,[21] HD,[22] and O_2[23] are used as standards. For intensity calibration, accurate polarizability anisotropy calculated by us previously[24,25] is used to determine the intensities of the rotational Raman bands of H_2, HD, and D_2 as intensity standards. Vibration–rotation Raman intensities of O_2 corrected for vibration–rotation interactions[26] are also used as additional intensity standards. Owing to large rotational constants, the hydrogen isotopologues yield a number of pure rotational Raman bands that span a broad spectral range. Combination of these data with the vibration–rotation bands of O_2 allows us to calibrate the spectral range of −1,036 to 1,700 cm^{-1} in relative wavenumbers, both for wavenumber position and intensity with high accuracy. The parallel and perpendicular Raman intensities are separately measured, and the intensity calibration is performed for each of the polarization components.

We validate the accuracy of the performed calibration by error estimation in the intensity determination and its propagation to the eventual instrument response function. The accuracy is further validated by temperature determination using the anti-Stokes to Stokes intensity ratios and by the polarized measurements of polarized and depolarized bands with known depolarization ratios. Finally, accurate Raman spectra of liquid samples of carbon tetrachloride, benzene, cyclohexane, toluene, and benzonitrile are given as a practically important outcome of the performed calibration. They are suitable for use as secondary standards for straightforward intensity calibration with accuracies better than 5%. Updated values of the vibrational frequencies of indene are included for

routine wavenumber calibration of Raman spectrometers. A set of programs developed during the current study using least squares minimization to perform wavenumber and intensity calibration from the observed Raman intensities of the four gases employed in the present work have been made available on GitHub.[27]

2 | APPROACH

The present approach for calibration is based on the application of accurate theoretical transition wavenumbers and intensities of the standards (H_2, D_2, HD, and O_2), which have been critically compared with experimental results.

For wavenumber calibration, the transition wave numbers for H_2 and D_2 have been obtained from the accurate theoretical rovibrational energy states calculated using nonadiabatic potential reported by Komasa et al.[21] For HD, analogous values have been taken from the work of Pachucki and Komasa.[22] Experimental results by Edwards et al.[23] have been used for the transition wavenumbers for O_2 up to $J = 17$. For higher J states, transition wavenumbers have been theoretically determined by solving the radial nuclear equation for the rovibrational states of different isotopes of O_2 in the ground electronic state, employing the theoretical potential reported by Bytautas et al.[28] (see Table S7, Section 4 in the Supplementary Material for tabulation of transition wavenumbers and correction factors for pure rotation and for the O1- and S1-branches of O_2 up to $J = 17$).

Correction for intensity begins with the correction to obtain the number of photons per wavenumber, which are initially measured over an approximately linear wavelength scale.[29–32] Measured Raman spectra have been corrected using a multiplicative factor, $(\delta\nu_s/\delta\nu_0)$, which is equal to $\left(\frac{\nu_s}{\nu_o}\right)^2\left(\frac{\delta\lambda_s}{\delta\lambda_o}\right)$, where ν_s and ν_o correspond to absolute wavenumbers across the wavenumber axis and a reference wavenumber, respectively. $\delta\lambda_s$ and $\delta\lambda_o$correspond to wavelength spacing per channel and the wavelength spacing per channel at the reference wavenumber, ν_o. In the present case, the reference in absolute wavenumbers, ν_o, is the wavenumber of the laser used. It is emphasized that this correction is necessary for obtaining vibrational spectra as photons/wavenumber, which is otherwise measured as photons/wavelength or photons/channels. Details including plots of the correction mentioned above are given in Section 1 in the Supplementary Material.

In the next step, a white light lamp is used as a broadband light source for correcting the channel-to-channel variations in the sensitivity incurred in multichannel detection. This step is required because the rotational Raman bands from H_2 and its isotopomers are sparsely spaced and provide information about the sensitivity only at these sparse positions (in wavenumber/wavelength). High temperature lamps can be assumed in the first approximation to be black-body emitters providing broadband white light spectra, whose photon counts per unit solid angle, per unit wavenumbers expressed as $I(\omega, T)$, is given by

$$I(\omega, T) = 2c\omega^2\left(\frac{1}{e^{hc\omega/k_BT} - 1}\right). \quad (1)$$

A rough approximation to the actually observed broadband spectra, W_{obs}, can be made using Equation 1 and the temperature, T, as a variable, to obtain $f(T)$ as a fit. W_{obs} divided by $f(T)$ yields the first correction curve, denoted as $C_1 = W_{\text{obs}}/f(T)$, which contains information about the channel-to-channel sensitivity of the spectrometer. This function is used as the next correction for intensity in the target spectra and is expected to contain significant error because the used light source may not behave as a true black-body emitter, its temperature is only assumed, and any information regarding the polarization-dependent sensitivity is lacking.

In the final step, rotational Raman intensities from gases are used to determine the final correction curve, which effectively corrects for any inconsistencies/errors introduced in the earlier rounds of correction. Rotational Raman intensities for diatomic molecules[33,34] are given by

$$I = S(\tilde{\nu}_{v,J\to v',J\pm2})I_oNF_J\sigma_{J\to J\pm2}, \quad (2)$$

where $S(\tilde{\nu}_{v,J\to v',J\pm2})$ is the wavelength-dependent sensitivity of the spectrometer, I_o is the incident laser intensity, N is the number of molecules, F_J is the fractional population of the molecules in the rotational state J, and $\sigma_{J\to J\pm2}$ is the effective Raman cross-section for the $J \to J \pm 2$ transition measured through an experimentally fixed solid angle. The fraction of molecules populating the J-level is governed by the Boltzmann population including the nuclear spin and is dependent on temperature.

Taking a ratio of the rotational Raman intensities originating from a common rotational state eliminates the term for relative population and removes the temperature dependence to give

$$\frac{I_{v,J\to v',J+2}}{I_{v,J\to v',J-2}} = \frac{S(\tilde{\nu}_{v,J\to v',J+2})\sigma_{v,J\to v',J+2}}{S(\tilde{\nu}_{v,J\to v',J-2})\sigma_{v,J\to v',J-2}}. \quad (3)$$

Expanding the Raman cross-section term yields

$$\frac{I_{v,J\to v',J+2}}{I_{v,J\to v',J-2}} = \frac{S(\tilde{\nu}_{v,J\to v',J+2})}{S(\tilde{\nu}_{v,J\to v',J-2})} \frac{b^{(2)}_{J\to J+2}}{b^{(2)}_{J\to J-2}} \frac{(\tilde{\nu}_0 - \tilde{\nu}_{v,J\to v',J+2})^3}{(\tilde{\nu}_0 + \tilde{\nu}_{v,J\to v',J-2})^3} \frac{\langle\gamma\rangle^2_{v,J\to v',J+2}}{\langle\gamma\rangle^2_{v,J\to v',J-2}}, \tag{4}$$

where $b^{(2)}_{J\to J+2}$ and $b^{(2)}_{J\to J-2}$ are the Placzek–Teller factors, $\tilde{\nu}_0$ is the frequency factor comprising the laser frequency, and $\langle\gamma\rangle^2_{v,J\to v',J\pm2}$ is the square of the polarizability anisotropy matrix element connecting the initial state v,J to the final state v',$J \pm 2$. The last term involving the square of the polarizability anisotropy matrix element, also referred to as the vibration–rotation correction factor,[31,32] accounts for the change in the Raman cross-section over rotational states.

Simplification of Equation 4, assuming the relative wavelength-dependent sensitivity, $S(\tilde{\nu}_{v,J\to v',J\pm2})$, as a polynomial, produces

$$\frac{I_{v,J\to v',J+2}/I_{v,J\to v',J-2}}{\frac{(J+1)(J+2)(2J-1)}{J(J-1)(2J+3)} \frac{(\tilde{\nu}_0 - \tilde{\nu}_{v,J\to v',J+2})^3}{(\tilde{\nu}_0 + \tilde{\nu}_{v,J\to v',J-2})^3} \frac{\langle\gamma\rangle^2_{v,J\to v',J+2}}{\langle\gamma\rangle^2_{v,J\to v',J-2}}} = \frac{1 + \sum_i c_i \tilde{\nu}^i_{v,J\to v',J+2}}{1 + \sum_i c_i \tilde{\nu}^i_{v,J\to v',J-2}}, \tag{5}$$

where the numerator and denominator on the left-hand side (LHS) correspond to the ratio of experimental intensities and the ratio of Raman cross-sections for rotational transitions from the common rotational state, respectively. The coefficients c_i in Equation 5 are obtained by expanding the wavelength-dependent sensitivity, $S(\tilde{\nu}_{v,J\to v',J\pm2})$, into a polynomial in $\tilde{\nu}$ and by a nonlinear least squares minimization to all $J \pm 2$ pairs of experimental Raman data for H_2, HD, D_2, and O_2. The residual function used is given as

$$\text{Residual} = \sum_k w_k (\text{LHS} - \text{RHS})^2, \tag{6}$$

where w_k is the weight for the specific pair of rotational Raman band derived from the error in the experimental intensities.

Equations 4 and 5 require the knowledge of the ratio of square of polarizability anisotropy for specific pairs of transitions originating from a common rotational state. We calculated the wavelength-dependent matrix elements of polarizability anisotropy for H_2, HD, and D_2 with high accuracy (error <0.1%) in our previous work.[24,25] In the present experiment, we utilize 13 pairs of pure rotational Raman bands from H_2, HD, and D_2 (in the range from −1,034 to 1,447 cm^{-1}), for which the required ratios of square of polarizability anisotropy are available. For O_2, we use the vibration–rotation Raman bands (O1- and S1-branches) accompanying the fundamental in the 1,400–1,700 cm^{-1} region, for which the corresponding ratio of polarizability anisotropy matrix elements has been reported by Buldakov et al.[26] This inclusion of vibration–rotation bands from O_2 helps us to extend the calibration region while improving accuracy for both wavenumber and intensity calibration on the Stokes end of the Raman spectra where bands from H_2, HD, and D_2 are weak.

Refer to Section 2 of the Supplementary Material and the online available programs[27] written for Igor Pro[35] and Python,[36] for details on the implementation and benchmarking of the fitting procedures mentioned above.

3 | EXPERIMENTAL

A laboratory constructed confocal Raman microspectrometer operating with a stabilized 532-nm laser (CW Nd:YVO_4; Verdi-V5, Coherent) has been used for experiments (Figure 1). The laser wavelength has been stabilized using a high-resolution wavelength meter (WS-7, HighFinesse) along with a piezo controller at 18,789.985 (±0.003) cm^{-1}. The excitation beam has been directed into an inverted microscope (iX71, Olympus) after passing through a Faraday isolator, laser line filter, and a linear polarizer (Glan–Taylor prism). A long working distance objective (20×, NA 0.25, f = 25 mm, Olympus SLMPLN20x) has been used to focus laser beam inside the sample. Laser power of around 200 mW for gases and 0.3 mW for liquids has been used. Backscattered light collected using the same objective lens passed through confocal setup consisting of a 100-μm pinhole. After the confocal setup, Rayleigh scattering has been removed using three volume Bragg notch filters (OptiGrate), followed by Glan–Thompson polarizer (GTH10M-A, Thorlabs) on a rotation mount used as analyzer. Parallel or perpendicularly polarized beam selected using the analyzer has been focused on the polychromator slit (f = 50 cm, f/6.5, 600 gr/mm grating, SP-2500i, Princeton Instruments, slit width = 120 μm) using an achromatic convex lens, allowing for detection of parallel or perpendicularly polarized Raman spectra. Spectral resolution has been determined to be ~3.5 cm^{-1}. Spectra have been recorded using a Peltier-cooled charge-coupled device (CCD; DU970N-BV, Andor) with optimized settings for obtaining spectra with minimal noise.

The sample chamber for gases is a laboratory designed custom-built gas cell made of quartz equipped with resistance-based heater allowing to be heated up to ~620 K (Figure 1). This gas cell has been mounted on a poly(tetrafluoroethylene) adapter, enabling fixed placement on the microscope. The gas cell has been connected to a vacuum manifold allowing for removal of air and

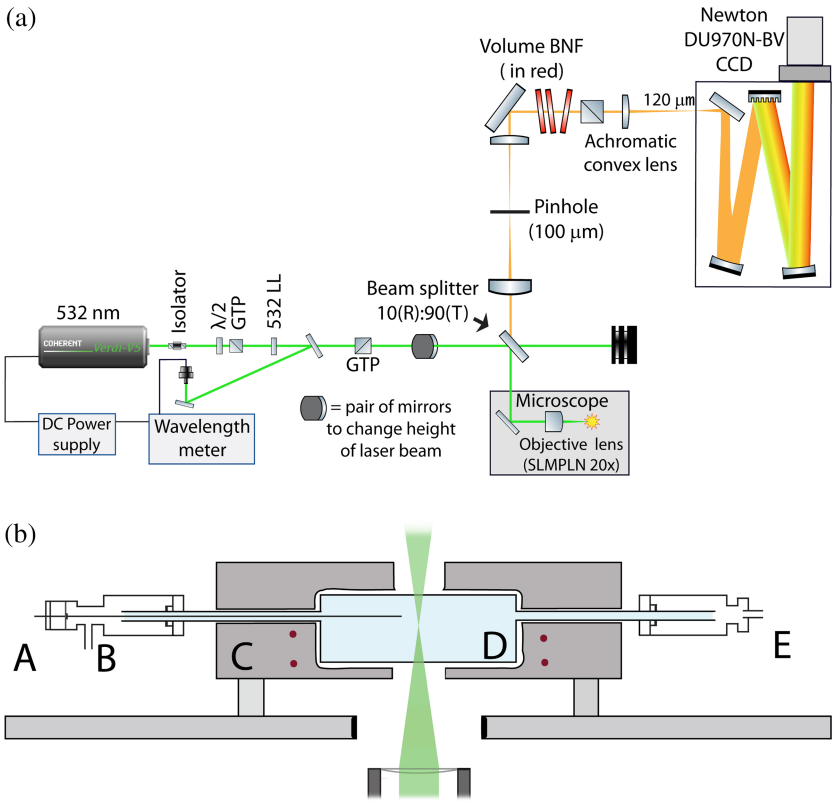

FIGURE 1 Layout of the Raman spectrometer used in the present work: (a) Overall view from the top where GTP refers to Glan–Taylor prism, 532 LL is the laser line filter for 532 nm, and volume BNF refers to volume Bragg notch filters (OptiGrate). Gas samples have been measured using a gas cell assembly placed on the microscope stage; (b) the gas cell assembly where (A) thermocouple inlet for measurement of temperature inside the cell, (B) inlet port for gases, (C) metal casing with resistive heaters, (D) quartz cell, and (E) inlet port for gases and/or vacuum manifold. Abbreviations: DC, direct current; CCD, charge-coupled device [Colour figure can be viewed at wileyonlinelibrary.com]

filling with hydrogen or other gases. Absolute pressure of the gas has been measured using a high-resolution pressure transducer (Omega PX409, National Institute of Standards and Technology [NIST] calibrated).

H_2 (Chiah Lung, Taiwan; 98% purity) and D_2 (Sigma-Aldrich, 99% purity) gases have been used in ~1:1 quantity, at a total pressure of ~3.6 atm, to generate an equilibrated mixture of H_2, HD, and D_2 by using elevated temperature (~570 K) over a period of 14 h. O_2 (Chiah Lung, Taiwan; 99% purity) has been measured separately at around 3.5 atm. All gases have been measured at room temperature. Separate Raman measurements of the gases at 0.6 atm for all gases have been performed to check effects on the band position and relative Raman intensities.

Raman spectra of the following liquid samples have been measured in a quartz cuvette, without further purification, at room temperature: deionized water (Merck Millipore), carbon tetrachloride (99%, Acros Organics), cyclohexane (99.5%, Sigma-Aldrich), benzene (99.5%, TCI Chemicals), toluene (99.8%, Acros Organics), and benzonitrile (99%, Sigma-Aldrich). Raman spectra of indene (99%, Sigma-Aldrich) have been measured in a quartz

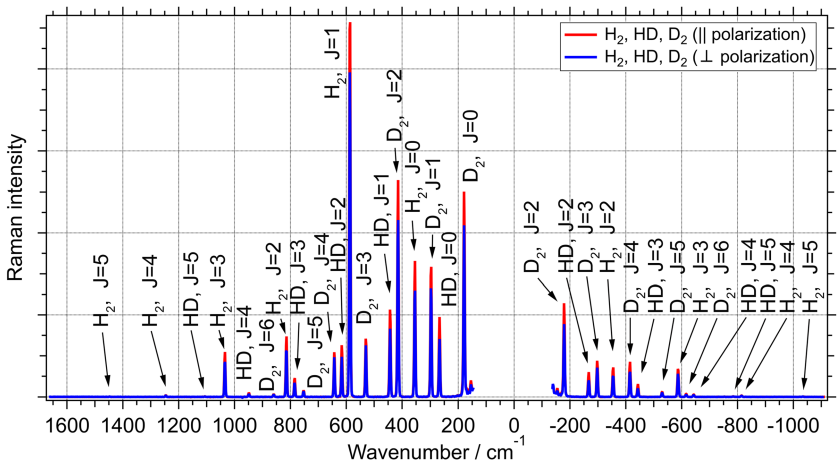

FIGURE 2 Pure rotational Raman spectra of H_2, HD, and D_2 with parallel and perpendicular polarization. These spectra are partially intensity corrected, and the perpendicularly polarized spectra are not corrected for polarization-dependent sensitivity. The perpendicularly polarized spectra are expected to have intensities corresponding to 75% to those of parallel spectra, but in reality, lower intensities are observed [Colour figure can be viewed at wileyonlinelibrary.com]

cuvette after distillation and degassing under argon. Broadband light spectra have been measured using a tungsten lamp (LS-1-CAL, Ocean Optics) placed on the microscope stage.

4 | RESULTS AND DISCUSSION

4.1 | Wavenumber calibration

Wavenumber calibration has been performed using 45 pure rotational Raman bands from H_2, HD, and D_2 covering the spectral range from −1,034 to 1,246 cm^{-1} and selected bands from O_2 in the wavenumber region of 1,400–1,700 cm^{-1} (Figures 2 and 3). After subtracting the background, which includes the dark counts, the band positions of the observed Raman bands on the CCD in pixel (including the error) have been determined using band fitting. Reference transition wavenumbers for H_2,[21] HD,[22] and D_2[21] have been obtained from accurate theoretical calculations with uncertainties less than 0.002 cm^{-1}. For O_2, these were taken from experimental work[23] having maximal uncertainty of 0.009 cm^{-1}. A tabulation of the relevant transition wavenumbers is given in Table 1. Least squares fitting, which included reciprocal of error as weights for both the pixel position and the reference Raman transition wavenumbers, has been performed using ODRPACK95[37–39] implemented in Igor Pro[35] and Python.[36] Fit for data set corresponding to parallel polarization is shown in Figure 4. For similar fit corresponding to perpendicular polarization, refer to Figure S14. Obtained residuals in both x and y axes have been converted to maximal error, 3σ, in the wavenumber calibration, which was 0.24 and 0.34 cm^{-1} for parallel and perpendicular polarization, respectively. See Section 5 in the Supplementary Material for details. The accuracy of the calibration has been checked by comparing the wavelengths of measured neon emission spectrum to reference vacuum wavelength data from NIST.[7] The net uncertainty in the wavelength of neon lines when using present calibration is ±0.009 nm or ±0.3 cm^{-1}, which includes additional uncertainty due to band fitting of the neon bands.

4.2 | Intensity calibration

Intensity calibration procedure employed in the present work is composed of three corrections: first, to obtain the spectra as photons/wavenumber, followed by the correction for pixel-to-pixel variation in the detector sensitivity, and finally, minor but crucial correction to the spectra, obtained from the fitting of the observed Raman intensity ratios to the theoretical primary standard.

First, contribution from the quartz window was removed from the target Raman spectra of the gases by a direct, one-to-one subtraction of the background spectra, which was measured from the evacuated cell. Spectra were then multiplied with a factor $\left(\frac{\nu_s}{\nu_o}\right)^2\left(\frac{\delta\lambda_s}{\delta\lambda_o}\right)$ to convert the intensity to photons/wavenumber. Next, the spectra were divided by the continuous correction curve, obtained from the broadband white light spectra (W_{obs}) and its fit $f(T)$ using Equation 1, shown in Section 6 of the Supplementary Material, in order to cancel the pixel-to-pixel variation in the sensitivity of the multichannel CCD detector.

In order to determine the final correction factor, the band areas of the rotational Raman bands of H_2, HD, and D_2 were obtained using band fitting. For O_2, the band areas of the O1- and S1-branches were determined by band fitting assuming Voigt function. The obtained experimental band intensities along with the theoretical Raman cross-sections were used in Equation 6 assuming the polynomial functions for the final correction. Nonlinear least squares minimization of Equation 6

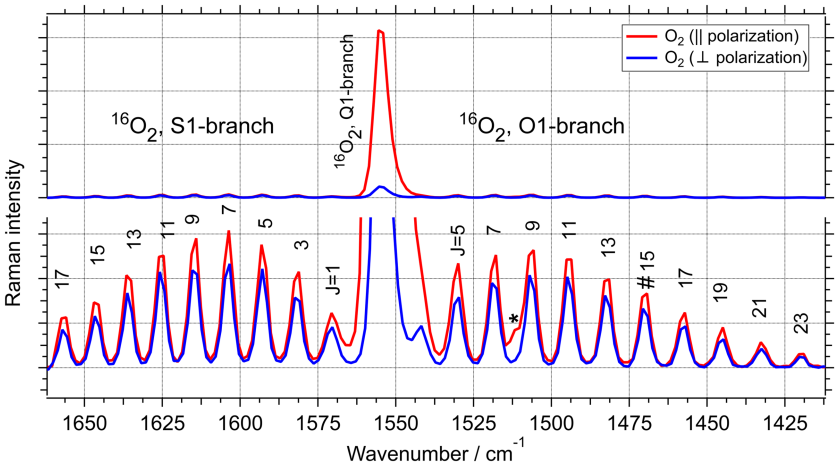

FIGURE 3 Measured parallelly and perpendicularly polarized spectra of $^{16}O_2$ showing the O1-, Q1-, and S1-branches. Small contribution from Q1-branch of $^{17}O_2$ at 1,510.5 cm^{-1} is designated with a star. Contribution from Q1-branch of $^{18}O_2$, designated with "#" at 1,468.4 cm^{-1}, is superimposed with the O1($J = 15$) band of $^{16}O_2$ [Colour figure can be viewed at wileyonlinelibrary.com]

TABLE 1 Transition wavenumbers, $\tilde{\nu}_{\text{Stokes}}$ and $\tilde{\nu}_{\text{anti-Stokes}}$, ($\text{cm}^{-1}$) and vibration–rotation correction factors, $F^{\gamma}_{0,0}(J)$ and $F^{\gamma}_{1,0}(J)$, for Raman transitions from a common rotational state for H_2, HD, D_2, and O_2, used in the present analysis

Molecule	J	$\tilde{\nu}_{\text{anti-Stokes}}$	$\tilde{\nu}_{\text{Stokes}}$	$F^{\gamma}_{0,0}(J)$[a]
H_2	2	−354.373	814.424	1.0379
	3	−587.032	1,034.671	1.0529
	4	−814.424	1,246.100	1.0677
	5	−1,034.671	1,447.281	1.0822
HD	2	−267.069	616.093	1.0287
	3	−443.081	785.002	1.0401
	4	−616.093	948.799	1.0514
	5	−785.002	1,106.582	1.0624
D_2	2	−179.067	414.649	1.0194
	3	−297.534	529.900	1.0271
	4	−414.649	642.807	1.0347
	5	−529.900	752.920	1.0423
	6	−642.807	859.832	1.0497
	7	−752.920	963.180	1.0569
Molecule	J	$\tilde{\nu}_{O1}$	$\tilde{\nu}_{S1}$	$F^{\gamma}_{1,0}(J)$[b]
O_2	7	1,518.537	1,603.819	0.94673
	9	1,506.632	1,614.635	0.92812
	11	1,494.622	1,625.316	0.90991
	13	1,482.486	1,635.857	0.89211
	15	1,470.239	1,646.252	0.87471
	17	1,457.878	1,656.511	0.85772
	19	1,445.408	1,666.620	0.84113

Note: Transition wavenumbers for H_2, HD, and D_2 have been taken from Komasa et al.[21] and Pachucki and Komasa[22] and have uncertainties of less than 0.002 cm^{-1}. Transition wavenumbers for O_2, J = 7–17, were taken from Edwards et al.[23] and have error less than 0.009 cm^{-1}. For J = 19 of O_2, potential function from Bytautas et al.[28] was used to compute the energies of rovibrational states in O_2, from which the Raman transition wavenumber was obtained, having maximal error of around 0.14 cm^{-1}.

[a] $F^{\gamma}_{0,0}(J) = \frac{\langle\gamma\rangle^2_{0,0\to 0,J+2}}{\langle\gamma\rangle^2_{0,J\to 0,J-2}}$ from Raj et al.[24,25]

[b] $F^{\gamma}_{1,0}(J) = \frac{\langle\gamma\rangle^2_{0,0\to 1,J+2}}{\langle\gamma\rangle^2_{0,J\to 1,J-2}}$ from Buldakov et al.[26]

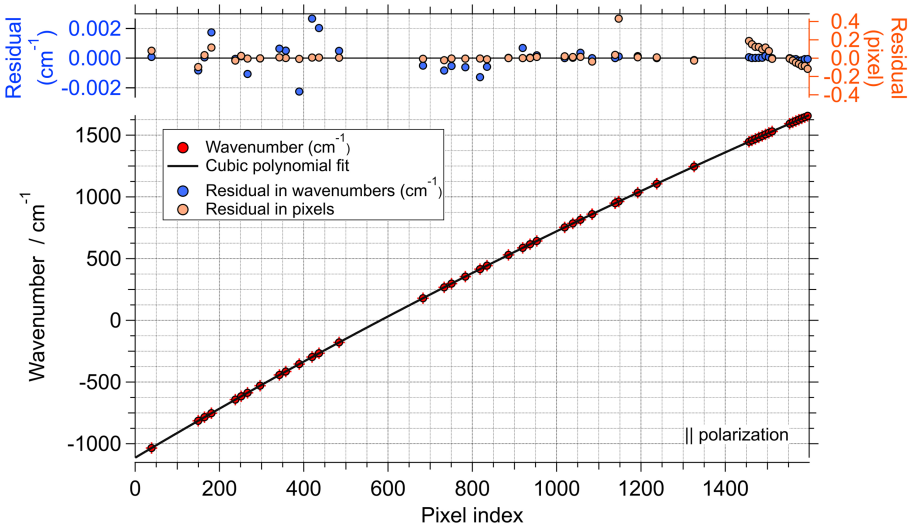

FIGURE 4 Cubic fit of accurate positions of Raman signals (in wavenumbers) to the corresponding observed band positions in pixels for wavenumber calibration using pure rotational Raman bands from H_2, HD, and D_2 and vibration–rotation bands from O_2 for parallel polarization. A total of 45 data points have been used (31 coming from H_2, HD, and D_2; 14 from O_2) [Colour figure can be viewed at wileyonlinelibrary.com]

was performed to obtain the fit coefficients. Fitting for parallel polarization using a total of 20 pairs of bands (four from H_2 and HD, five from D_2, and seven from O_2) is shown in Figure 5. Refer to Figure S14 for the corresponding fit for data from perpendicularly polarized spectra. Weight factors for band pairs used in the fit were obtained considering the uncertainty in intensity of each of the bands and using error propagation (see Equation 7 for details on error estimation). The weight factors of bands from O_2, in the O1- and S1-branches, were significantly small (around 100 times smaller as compared with those of H_2 in our experiments) due to low intensities. In order to improve the contribution of data from O_2 in the fitting process, the band weights for O_2 were scaled by a uniform factor of 10. Overall, the data points from O_2 were given lower weights due to lower Raman intensities and possibly larger uncertainty in the vibration–rotation correction factors, which are wavelength independent, compared with H_2 and isotopologues. The net weights applied to the bands from the four gases during the fitting are shown in Section 3 of the Supplementary Material. The obtained polynomial functions representing the final correction for the Raman intensities for parallel and perpendicular polarization are shown in Figure S11 along with the details showing convergence of the fits and residuals. These functions have been used to perform the final correction to the Raman intensities of gases and liquid samples (water, carbon tetrachloride, cyclohexane, benzene, toluene, and benzonitrile).

Pressure broadening and the shift in band positions of rotational Raman bands for H_2, HD, and D_2 were studied earlier.[40,41] No appreciable shifts in the band positions were observed in our experiments, when comparing results from measurements at 0.6 and 3.6 atm, presumably because of the low spectral resolution and relatively low pressures. No changes of Raman intensity ratios were found either. Therefore, the obtained final wavelength-dependent sensitivity curves and subsequent results are pressure independent.

4.3 | Error estimation for band intensities and weights for the fit

In the process of calibration, we include very strong bands (e.g., bands within 200–600 cm^{-1}) and very weak bands (e.g., bands in the region over 1,100 cm^{-1}).

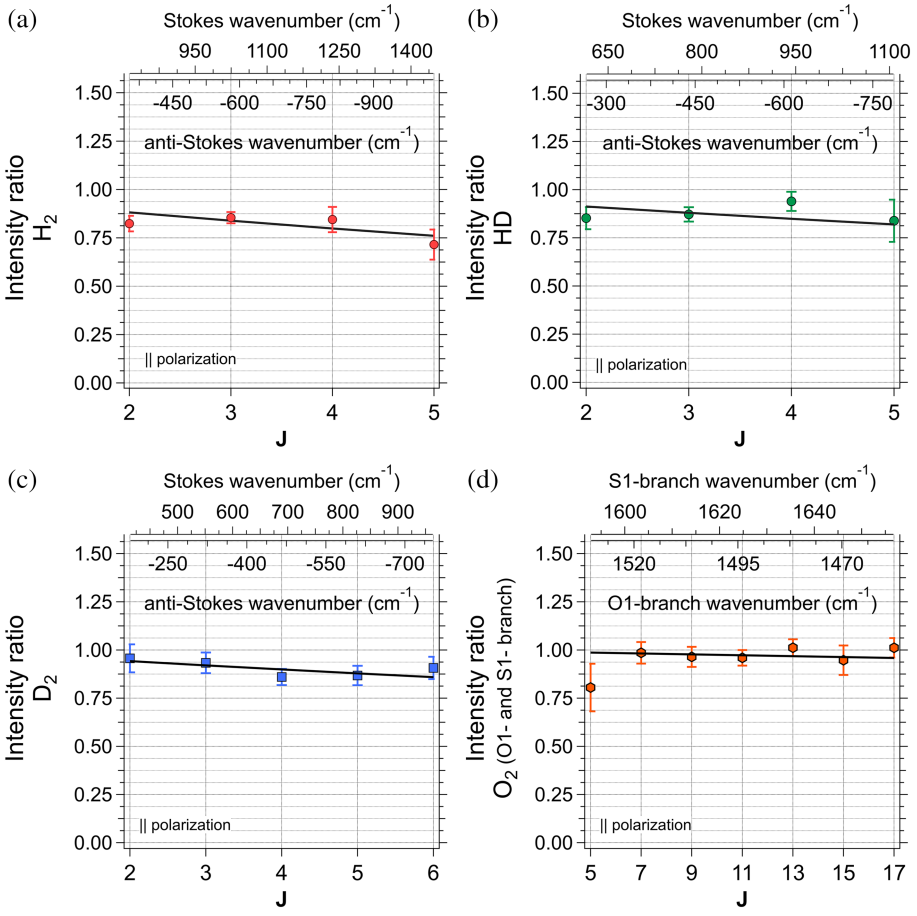

FIGURE 5 Fit of intensity ratios for H_2, HD, D_2, and O_2, where intensity ratio refers to the ratio of experimental intensities (Stokes to anti-Stokes, experimental) to theoretical intensities (Stokes to anti-Stokes, calculated). For O_2, the intensity ratio corresponds to similar ratio for S1(J) to O1(J), vibration–rotation bands. The intensity ratios constitute the left-hand side of Equation 5. The fits (black solid line) represent the ratio of the corresponding anti-Stokes and Stokes data points of the polynomial (obtained from fitting) and constitute the right-hand side of Equation 5 [Colour figure can be viewed at wileyonlinelibrary.com]

Because all of these bands are used for the determination of the wavelength-dependent sensitivity and its uncertainty, proper estimation of error for these band intensities becomes important. In order to correctly identify the error sources in the respective band intensities, we have performed an error estimation, which is described below.

Error in usual photon counting measurements comes from three primary sources: thermal noise of the photo detector; the shot noise coming from the uncertainty of the arrival of photons, both of which follow Poisson distribution; and lastly, the readout noise inherent to the digitization process and detector electronics. The net uncertainty in the counted photons is generally taken to be the $\sqrt{I}$, where I is the total counts, as a result of the Poisson distributions.

In the present work, we checked uncertainties in the band intensities by separately measuring the rotational Raman spectra of H_2 at varying exposures and repeating each measurement 56 times to obtain bands with varying signal-to-noise ratios. The experimental uncertainties in the band intensities of seven pure rotational Raman bands were determined as the 3σ corrected standard deviation having 99.7% confidence. The obtained 3σ corrected standard deviation versus the band intensity has been analyzed to obtain the actual estimates of experimental uncertainty, σ_{exp}. Estimates of error obtained using the square root were also compared. We found that the error estimated using the square root of the intensity was greater than the actual case by a few percent for high signal-to-noise ratio bands, and this trend reversed when going toward smaller signal-to-noise ratio bands. See Section 3 in the Supplementary Material for more details. Using the estimates of error obtained from above measurement, uncertainties of individual bands of H_2, HD, D_2, and O_2 for intensity calibration were determined. The weights for the fitting analysis (for determining the wavelength-dependent sensitivity) were computed as $w = 1/\sigma^2_{\text{total},i}$, where

$$\sigma_{\text{total},i} = \frac{I_{J+2}}{I_{J-2}}\sqrt{\left(\frac{\sigma_{\text{exp}}}{I_{J+2}}\right)_i^2 + \left(\frac{\sigma_{\text{exp}}}{I_{J-2}}\right)_i^2}, \tag{7}$$

for the i^{th} pair of bands involved. Magnitude of errors in the intensity ratios ranged from 1% for the most intense pairs of bands to 10% for the smallest bands, and about half of the total 21 intensity ratios used in the present analysis have errors below 5%. Specific values of weights obtained from these uncertainties are shown in Figure S6.

4.4 | Polarization correction

Pure rotational Raman bands from H_2, HD, D_2, and O1- and S1-branches of vibration–rotation bands of O_2 are depolarized, having depolarization ratio of 0.75.[33] It was however observed in our experiment that bands in the perpendicularly polarized spectra had intensities lower than 0.75 of the corresponding bands in the parallel polarization spectra (see Figures 2 and 3), very likely due to the polarization-dependent bias in the response of the optical components of the spectrometer including the polarizer and the analyzer. Experimental average depolarization ratio for total 52 bands from the analyzed gases was found to be 0.71 across the whole spectrum (Figure 6). This was obtained by fitting the observed depolarization ratio to a constant while including the reciprocals of errors as weights. Refer to Figure 6 for the plot of observed depolarization ratios from the 52 depolarized Raman bands and the corresponding fit. A ratio of the true to the observed depolarization ratio, computed as (0.75/0.71), has been

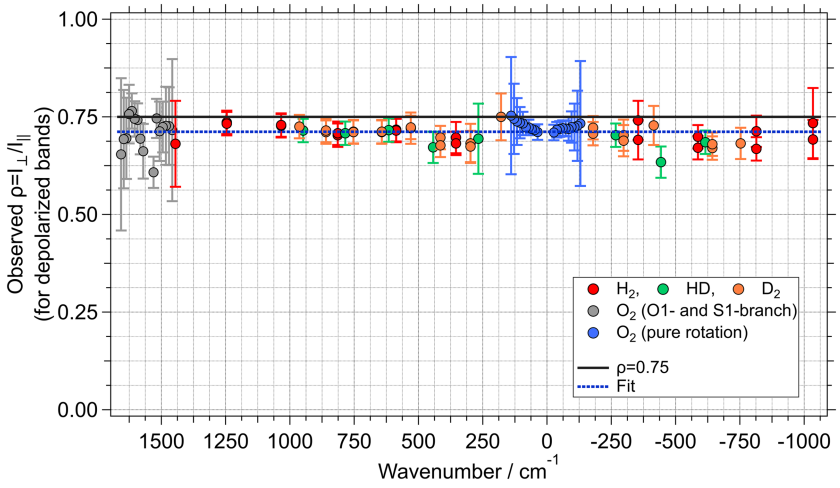

FIGURE 6 The observed ratios of perpendicular and parallel polarized Raman intensities for rotational bands of H_2, HD, D_2, and vibration–rotation bands of O_2. All of these bands are depolarized with an anticipated true depolarization ratio of 0.75 (represented as a black dashed line). This property is used for correcting the polarization dependence of the observed Raman intensities. The fit shown in broken blue line is used for obtaining the required correction for perpendicularly polarized spectra [Colour figure can be viewed at wileyonlinelibrary.com]

used for correcting the polarization dependence applicable for the perpendicularly polarized spectra.

4.5 | Validation

An independent assessment of the intensity correction procedure described here was performed on the basis of observed Raman intensities.

First test was conducted to estimate the accuracy of the corrected Raman intensities over the available wavenumber range, using the anti-Stokes and Stokes Raman intensities corresponding to the same vibrational levels. Ratio of the anti-Stokes and Stokes Raman intensities can be used to probe the temperature of the molecules in the focal volume.[33] This approach was used to test the correctness of the intensity calibration procedure across the covered wavenumber range by comparing the temperature obtained from the corrected spectra to the measured temperature on a thermocouple, for various vibrational Raman bands from different liquids. Water and organic liquids (carbon tetrachloride, cyclohexane, and benzene) were chosen as test samples. Using low wavenumber vibrational modes of water and prominent bands in the fingerprint region of the selected organic liquids, wavenumber range of 50–992 cm^{-1} has been checked, both in the Stokes and anti-Stokes regions and for both parallel and perpendicularly polarized spectra. Three independent Raman measurements of water were performed using a flow cell setup with 8-mW laser power. Organic liquids were measured in five independent experiments using a quartz cell with 0.4-mW laser power. All measurements were made at room temperature. Spectra were acquired after around 15 mins of laser irradiation on the sample for thermal equilibration. Temperature of the sample was separately measured using a K-type thermocouple with uncertainty of ±0.7 K during the course of the experiment. Parallel polarized low frequency Raman spectrum of water and the obtained temperature is shown in Figure 7. Corresponding figure for perpendicularly polarized spectra is shown in Figure S16. Broad features in the low frequency Raman spectra of water provide means for temperature determination using Raman intensities at multiple transition wavenumbers in the probed spectral range of 50–300 cm^{-1}. Temperatures determined from all these spectral points have been averaged for comparison with measured temperature using thermocouple, and the differences have been analyzed. The maximum absolute difference observed over three independent experiments is reported in Table. 2. Expected anti-Stokes to Stokes intensity ratios have been calculated using the thermocouple temperature, and these values are compared with the ratios obtained directly from the spectra, and the relative differences (in %) are calculated. For organic liquids, similar analyses as mentioned above were performed while analyzing five independent experiments. Tabulation of the analyzed specific Raman transition, approximate mode assignments given originally by Shimanouchi[42] for organic liquids and by Walrafen[43] for water; differences from the measured temperature and the percent differences in the Raman anti-Stokes to Stokes intensity ratios are tabulated in Table 2.For water, the analyzed spectral range is 50–300 cm^{-1}, with the mean temperature

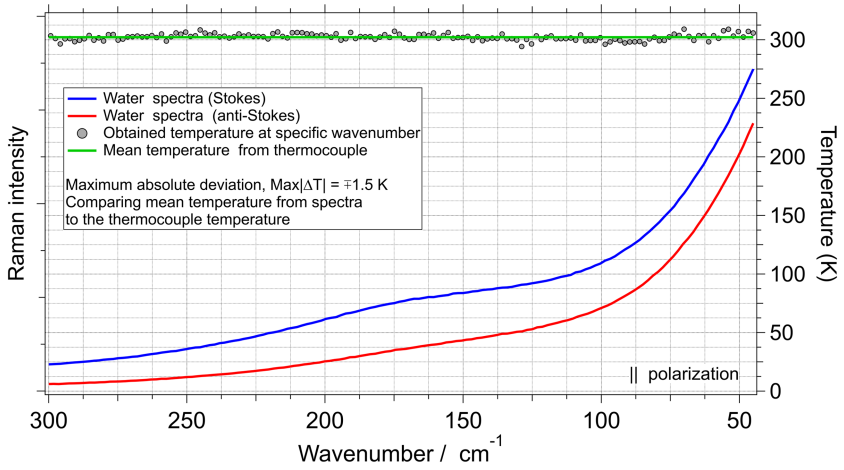

FIGURE 7 Comparison of temperatures determined for liquid water using the anti-Stokes to Stokes ratio in the low frequency region. The temperatures determined from spectra at specific wavenumbers are shown in gray circles. Mean temperature measured using a thermocouple during the spectra acquisition is shown as a green horizontal line. Comparison of average temperature from all the spectral data points (computed from anti-Stokes to Stokes Raman intensities) and mean temperature from thermocouple was performed to obtain the deviation. Maximum deviation in three independent experiments was found to be ±1.5 K for parallel polarization [Colour figure can be viewed at wileyonlinelibrary.com]

TABLE 2 Deviation in temperatures obtained from anti-Stokes to Stokes intensity ratios from Raman spectra to the measured temperature from thermocouple and the depolarization ratio of Raman bands from selected chemicals after intensity correction

	Transition (cm^{-1})		|| Polarization		⊥ Polarization		Depolarization ratio	
Molecule[a]	Mode[b]	$\tilde{\nu}$	Max$\|\Delta T\|$, K[c]	ΔI, %[d]	Max$\|\Delta T\|$, K[c]	ΔI, %[d]	Reference	Present
H_2O	Intermolecular vibrations	50–300	1.5	0.8	1.6	0.8		
CCl_4	Deg. deformation, *e*	218.1	1.1	0.4	1.2	0.4	0.75[e]	0.759 (0.015)
	Deg. deformation, *f* 2	313.9	1.2	0.7	1.8	0.9	0.75[e]	0.755 (0.014)
	Symmetric stretch, *a*1	460.2	1.1	0.8	2.2	1.7	0.0023[e]	0.028 (0.002)
							0.0065[f]	
C_6H_{12}	CC stretch, *a*1*g*	801.3	0.9	1.2	2.2	2.8		0.082 (0.006)
	CH_2 twisting, *eg*	1266.1					0.749 (0.002)[g]	0.759 (0.022)
	CH_2 scissoring, *eg*	1,443.7					0.750 (0.002)[g]	0.746 (0.020)
C_6H_6	Ring deformation, *e*2*u*	607	1	0.9	1.2	1.2		0.749 (0.021)
	Ring stretch, *a*1*g*	992.3	1.1	1.8	2	3.2	0.030 (0.002)[h]	0.055 (0.005)

[a]Natural isotopic mixture of the liquids was used.
[b]Mode assignments of organic liquids from Shimanouchi.[42] For water, the intermolecular bands were described in Walrafen.[43]
[c]Absolute maximum difference from the true temperature (measured using thermocouple) over five independent experiments.
[d]Difference, in percent, between the true anti-Stokes to Stokes ratio versus the one obtained from experiment. This is obtained as the percent difference between LHS and RHS of the equation, $\frac{I(\text{anti-Stokes})}{I(\text{Stokes})} \times \frac{(\tilde{\nu}_o - \tilde{\nu})^3}{(\tilde{\nu}_o + \tilde{\nu})^3} = e^{\frac{-hc\tilde{\nu}}{kT}}$, which is used to determine the temperature from anti-Stokes and Stokes Raman intensities.
[e]Kiefer and Topp.[44]
[f]Chantry[45] and Fukushi and Kimura.[46]
[g]Saito et al.[47]
[h]Fernández-Sánchez and Montero.[48]

computed from all the available spectral data points in this range. Maximum deviations in temperature of 1.5 K for parallel polarization and 1.6 K for perpendicular polarization were detected in three independent experiments. In terms of the deviation in the anti-Stokes to Stokes intensity ratio, the difference has been found to be <0.8% for this spectral range. Figure 7 shows the low frequency Stokes and the corresponding anti-Stokes Raman spectra of water with the temperature obtained using the anti-Stokes to Stokes ratio. Consistency of the determined temperature across the whole spectrum signifies the high accuracy of the Raman spectra obtained using the intensity calibration procedure. Raman bands in the fingerprint region coming from CCl_4, C_6H_{12}, and C_6H_6 in the spectral range of 218–992 cm^{-1} indicate fairly accurate temperature determination with maximum difference of 1.2 K for the parallel polarized spectra. Corresponding difference in the intensity ratio was <2% across the whole spectral range. Perpendicularly polarized spectra show larger temperature difference of up to 2.2 K, which is seen for the polarized Raman bands such as 460.2 cm^{-1} from CCl_4, 801.3 cm^{-1} from C_6H_{12}, and 992.3 cm^{-1} from C_6H_6. For these polarized bands, the difference in intensity ratios is up to 3%. Depolarization ratios show good correspondence to the previous more accurate results obtained using more specialized techniques.[44–48] Depolarized bands (having $\rho = 0.75$) show better agreement than the polarized bands due to smaller experimental errors associated with larger intensities in the perpendicularly polarized spectra. In general, the results in Table 2 indicate that the maximal error in the intensity calibration is around 2% over the covered −992 to 992 cm^{-1} range using anti-Stokes and Stokes bands for parallel polarization and around 3% for perpendicular polarization. Beyond 992 cm^{-1}, the accuracy is expected to be of similar quality because several closely spaced data points from O_2 in the 1,400–1,700 cm^{-1} were used during the intensity calibration procedure.

4.6 | Standard spectra of selected organic liquids

Employing the calibrated Raman spectrometer, measurements toward standard relative Raman intensities in five organic liquids have been performed, whose results are discussed here. Table 3 lists the transition wavenumbers for selected vibrational modes with assignments,[42,49–52]

relative intensities, and depolarization ratios together with the estimated errors for selected intense Raman bands in CCl_4, C_6H_{12}, C_6H_6, $C_6H_5CH_3$, and C_6H_5CN. Standard calibrated Raman spectra of these molecules are given in Section 9 of the Supplementary Material.

The reported Raman transition wavenumbers were determined by band fitting using either Gaussian, Lorentzian, or Voigt functions. See Tables S27 and S28 for details on fitting of each band. The error in transition wavenumbers is the net error obtained by combining uncertainties in the band position from the fit and the error introduced during wavenumber calibration. The maximum error observed in the set of five independent experiments is listed in Table 3. Relative Raman intensities have been determined by normalizing the band area, obtained from the fit, to the most intense band in the parallel polarized spectra of a given molecule. The error in relative intensities includes the uncertainties in band fitting, typically ≤1% combined with the estimated error in intensity calibration, around 1%–2%. The relative Raman intensities in Table 3 follow the Boltzmann distribution, enabling temperature determination from anti-Stokes to Stokes ratios, which provides another check for the accuracy of the Raman intensities as discussed earlier. Overall, the relative intensities have error <4% for the parallel polarized case. In the perpendicularly polarized measurements, the depolarized bands observed in the perpendicular polarization measurements have similar error profiles, whereas polarized bands show larger error due to significantly lower Raman intensities.

Comparisons of the perpendicular to parallel Raman intensities have been performed to obtain the depolarization ratios (ρ). These are listed for all the reported bands. As discussed earlier, the polarized bands ($\rho < 0.75$) have larger uncertainty in ρ, around 5%–10%, due to lower intensities in the perpendicularly polarized spectra, whereas the relatively intense depolarized bands ($\rho \approx 0.75$) have error of around 2%–3%.

The optical transmittance of the liquids and the gases used for intensity calibration differs. The effect of this difference is estimated to be small due to the small path length of scattered light in the optically transparent samples. Contribution of this difference, if detectable in the measured data, is within the uncertainties mentioned with the relative intensities of the liquids.

4.7 | Vibrational frequencies of indene for wavenumber calibration

Indene is frequently used for routine wavenumber calibration work.[3,4,53] Raman spectrum of indene has been measured on the present spectrometer, which was calibrated for wavenumber using the Raman bands of gases (described in Sec 4.1). Vibrational frequencies of indene determined using band fitting are listed in Table 4; 3σ uncertainty, which includes error from fitting and repeat measurements, is found to be around 0.4 cm^{-1}. A comparison with previous works shows good correspondence with the present updated values. The spectrum is shown in Section 10 of the Supplementary material.

5 | DISCUSSION

The use of pure rotation and vibration–rotation bands for calibration purposes has distinct advantages, like applicability for both wavenumber and intensity calibration, as demonstrated in the present work. Furthermore, Raman intensities from molecular hydrogen and its isotopologues serve as high accuracy independent standards, which can be compared with accurate theoretical Raman intensities determined using ab initio wavelength-dependent polarizability invariants and rovibrational wavefunctions.[19,24,25] Thus, high accuracy in wavenumber and intensity calibration can be realized due to the particularly simple quantum structure of H_2.

Transition wavenumbers of the gases are used for wavenumber calibration in the present work. These are useful for high-resolution Raman spectroscopy where the full potential of the high accuracy with the narrow observed linewidths can be utilized. For commonly used spectrometers, the wavenumber positions of organic liquids included in this work suffice as more practical wavenumber standards.

Conventional intensity calibration standards lack information about polarization-dependent response, which is intrinsically available when using rotational and vibration–rotation Raman intensities. The intensity calibration procedure described here is also applicable to other kinds of spectrometers like hyper-Raman, fluorescence,[54,55] and Thomson scattering spectrometers.[56,57]

Improvements in the present intensity calibration procedure over previously reported techniques utilizing rotational Raman intensity ratios are briefly discussed below. The present approach is similar in methodology to the earlier work by Hamaguchi et al.,[18] where D_2 was used to calibrate the spectral window of 455–529 nm (~3,075 cm^{-1} in relative wavenumbers assuming excitation at 488 nm) using five excitation lines from argon ion laser achieving error within 2%, and by Okajima and Hamaguchi[19] employing pure rotational Raman bands of N_2 to calibrate Raman spectral range from −150 to 150 cm^{-1} with high accuracy having error of 1% or less while using 532-nm excitation. In the present work, we have successfully employed rotation and vibration–

TABLE 3 Raman transition wavenumbers, relative Raman intensities, and observed depolarization ratios of selected vibrational bands of carbon tetrachloride, cyclohexane, benzene, toluene, and benzonitrile. Temperatures of the samples are noted below the table

	Transition				Relative intensity[a]				Depolarization ratio	
Molecule	Mode[b]	Irrep	$\tilde{\nu}^c$ (cm^{-1})	$\Delta\tilde{\nu}^d$	|| Polarization	Error[e]	⊥ Polarization	Error[e]	$\rho = I_\perp/I_{\|\|}$	Error
CCl_4	Sym. stretch (ν_1)	a_1	−460.2	0.7	0.12929	0.00220	0.00375	0.00010	0.029	0.002
	Deg. deform (ν_4)	f_2	−313.9	0.6	0.09165	0.00165	0.06865	0.00124	0.749	0.019
	Deg. deform (ν_2)	e	−218.1	0.6	0.12672	0.00230	0.09707	0.00176	0.766	0.020
	Deg. deform (ν_2)	e	218.1	0.6	0.33570	0.00400	0.25479	0.00304	0.759	0.013
	Deg. deform (ν_4)	f_2	313.9	0.6	0.37907	0.00500	0.28619	0.00378	0.755	0.014
	Sym. stretch (ν_1)	a_1	460.2	0.6	1.00000		0.02800	0.00100	0.028	0.002
	Fermi res. (ν_3, $\nu_1 + \nu_4$)	f_2	759.4	0.8	0.11554	0.00240	0.08770	0.00190	0.759	0.023
		f_2	789.6	0.8	0.13740	0.00275	0.10360	0.00220	0.754	0.022
C_6H_{12}	CC stretch (ν_5)	a_1g	−801.3	0.7	0.02709	0.00054	0.00222	0.00010	0.082	0.005
	CCC deform + CC torsion (ν_{24})	e_g	−426.0	0.6	0.00825	0.00040	0.00615	0.00030	0.745	0.051
	CCC deform + CC torsion (ν_6)	a_1g	−383.1	0.6	0.01279	0.00050	0.00180	0.00009	0.141	0.010
	CCC deform + CC torsion (ν_6)	a_1g	383.1	0.6	0.07087	0.00100	0.01035	0.00049	0.146	0.010
	CCC deform + CC torsion (ν_{24})	e_g	426.0	0.6	0.05824	0.00100	0.04357	0.00075	0.748	0.018
	CC stretch (ν_5)	a_1g	801.3	0.5	1.00000		0.08773	0.00100	0.088	0.003
	CC stretch (ν_{22})	e_g	1,027.7	0.5	0.41122	0.00822	0.30883	0.00618	0.751	0.021
	CH_2 rock (ν_4)	a_1g	1,157.3	0.6	0.08549	0.00200	0.02410	0.00056	0.282	0.010
	CH_2 twist (ν_{21})	e_g	1,266.1	0.6	0.35901	0.00718	0.27241	0.00545	0.759	0.021
	CH_2 wag (ν_{20})	e_g	1,346.5	0.7	0.07164	0.00200	0.05359	0.00150	0.748	0.030
	CH_2 scis. (ν_{19})	e_g	1,443.7	0.8	0.42878	0.00790	0.31974	0.00589	0.746	0.019
C_6H_6	Ring stretch (ν_2)	a_1g	−992.3	0.7	0.01161	0.00040	0.00068	0.00002	0.059	0.005
	Ring deform (ν_{18})	e_2g	−607.0	0.6	0.00342	0.00010	0.00262	0.00008	0.764	0.032
	Ring deform (ν_{18})	e_2g	607.0	0.6	0.05376	0.00108	0.04027	0.00081	0.749	0.021
	Ring stretch (ν_2)	a_1g	992.3	0.5	1.00000		0.05500	0.00100	0.055	0.005
	CH bend (ν_{17})	e_2g	1,176.5	0.6	0.08864	0.00240	0.06727	0.00182	0.759	0.029
	Fermi res. (ν_{16}, $\nu_2 + \nu_{18}$)	e_2g	1,585.5	0.7	0.06499	0.00220	0.04887	0.00165	0.752	0.036
		e_2g	1,606.7	0.7	0.03826	0.00180	0.02946	0.00139	0.770	0.051
$C_6H_5CH_3$	C═C stretch (ν_{10})	a_1	−1,030.3	0.7	0.00208	0.00010	0.00016	0.00001	0.076	0.008
	C═C stretch (ν_{11})	a_1	−1,003.3	0.6	0.01184	0.00040	0.00037	0.00001	0.031	0.008
	Φ-me stretch (ν_{12})	a_1	−786.0	0.6	0.01888	0.00038	0.00061	0.00010	0.033	0.008
	Φ-deform. (ν_{13})	a_1	−521.2	0.6	0.01760	0.00030	0.00537	0.00009	0.305	0.009
	Φ-deform. (ν_{13})	a_1	521.2	0.5	0.18309	0.00270	0.05596	0.00083	0.306	0.007
	Φ-me stretch (ν_{12})	a_1	786.0	0.5	0.59848	0.01197	0.01947	0.00039	0.033	0.004
	C═C stretch (ν_{11})	a_1	1,003.3	0.5	1.00000		0.03200	0.00100	0.032	0.003
	C═C stretch (ν_{10})	a_1	1,030.3	0.6	0.21367	0.00440	0.01624	0.00033	0.076	0.003
	CH bend (ν_{34})	b_2	1,155.6	0.9	0.05824	0.00160	0.04019	0.00110	0.690	0.032
	CH bend (ν_9)	a_1	1,179.1	0.9	0.04158	0.00090	0.03156	0.00068	0.759	0.029
	Φ-me stretch (ν_8)	a_1	1,210.0	0.6	0.28688	0.00620	0.01633	0.00035	0.057	0.003

(Continues)

TABLE 3 (Continued)

Molecule	Transition				Relative intensity[a]				Depolarization ratio	
	Mode[b]	Irrep	$\tilde{\nu}$[c] (cm^{-1})	$\Delta\tilde{\nu}$[d]	|| Polarization	Error[e]	⊥ Polarization	Error[e]	$\rho = I_{\perp}/I_{\|\|}$	Error
	Me sym deform. (ν_7)	a_1	1,379.3	0.8	0.09692	0.00220	0.03135	0.00080	0.323	
	C═C stretch (ν_{29})	b_2	1,585.3	0.8	0.06770	0.00260	0.04820	0.00200	0.712	0.040
	C═C stretch (ν_5)	a_1	1,605.3	0.8	0.12000	0.00420	0.09348	0.00400	0.779	0.043
C_6H_5CN	CC stretch (ν_9)	a_1	−1,026.6	1.0	0.00136	0.00010	0.00006	0.00002	0.043	0.015
	Ring deform (ν_{10})	a_1	−1,000.7	0.6	0.01174	0.00023	0.00057	0.00001	0.049	0.003
	Ring deform (ν_{31})	b_2	−624.7	0.7	0.00481	0.00010	0.00319	0.00007	0.663	0.020
	CCN linear bend with CC wag (ν_{20})	b_1	−548.6	0.6	0.00740	0.00020	0.00507	0.00014	0.685	0.026
	Ring deform with CC stretch (ν_{12})	a_1	−460.8	0.6	0.03003	0.00050	0.00556	0.00009	0.185	0.006
	Ring deform with CC stretch (ν_{12})	a_1	460.8	0.6	0.23437	0.00440	0.04279	0.00080	0.183	0.009
	CCN linear bend with CC wag (ν_{20})	b_1	548.6	0.6	0.08522	0.00160	0.05903	0.00111	0.693	0.018
	Ring deform (ν_{31})	b_2	624.7	0.7	0.07400	0.00175	0.05172	0.00122	0.699	0.023
	Ring deform (ν_{10})	a_1	1,000.7	0.5	1.00000		0.05127	0.00100	0.051	0.006
	C═C stretch (ν_9)	a_1	1,026.6	0.6	0.12672	0.00260	0.00543	0.00011	0.043	0.005
	C═C stretch (ν_5)	a_1	1,599.0	0.5	0.52194	0.01044	0.29535	0.00591	0.566	0.030

Note: Temperatures (K) recorded during the measurement: CCl_4 (298.6), C_6H_{12} (298.7), C_6H_6 (298.6), $C_6H_5CH_3$ (299.2), and C_6H_5CN (299.5), with error of ±0.7 K.

[a]Relative Raman intensities are normalized to the most intense band in the parallel polarized spectra.

[b]Mode assignments: CCl_4, C_6H_{12}, and C_6H_6 from Shimanouchi[42]; $C_6H_5CH_3$ from Tasumi et al.[49] and Hickman et al.[50] where ring is denoted as Φ; C_6H_5CN from Green and Harrison[51] and Császár and Fogarasi.[52]

[c]Obtained from band fitting.

[d]Error in transition wavenumber includes uncertainty in the band position obtained while fitting and the net error in wavenumber calibration. Maximum error observed in five independent experiments is given above.

[e]Error in relative intensities includes uncertainty in the band area (from fit), estimated error in the intensity calibration tested using anti-Stokes to Stokes ratio for temperature, and the error in band area of the most intense band used for normalization.

rotation bands from four gases while using a single excitation laser at 532 nm with total calibrated spectral range of around 2,736 cm^{-1}, measuring both parallel and perpendicular polarized spectra and still keeping the error within 2% for parallel polarized spectra and 2%–3% for perpendicularly polarized case. Schlösser et al.[20] directly compared experimental and theoretical intensities at certain temperatures and relative concentration of multiple hydrogen species to obtain the wavelength dependence. Comparatively, the present approach of using ratios of rotational Raman intensities does not require information regarding the relative concentrations (or pressures) of the multiple gases used, nor the temperature at the focal point. In addition, we introduce the correction for two polarization orientations using the rotational Raman bands and their known depolarization ratio of 0.75.

A major disadvantage of using rotation and vibration–rotation Raman bands is their small Raman cross-sections, thus requiring high laser powers combined with long exposures for obtaining high-quality Raman spectra. H_2 and its isotopologues also require careful handling and leak-proof gas measurement setup due to their explosive nature.

Accurate wavenumbers and relative intensities of organic liquids presented in Table 3 can also be used for both wavenumber and intensity calibration of Raman spectra, serving as commonly available laboratory standards.

TABLE 4 Vibrational frequencies of indene for wavenumber calibration

Our study		Hamaguchi[3]		Harada and Hiraishi[53]	
1,609.8	(0.4)	1,609.7	(0.3)	1,609.7	(0.5)
1,588.9	(0.5)	1,588.4	(0.4)	1,587.8	(1)
1,552.3	(0.4)	1,552.2	(0.5)	1,553.2	(1)
1,457.6	(0.3)	1,457.5	(0.4)	1,457.1	(1)
1,392.8	(0.3)	1,393.2	(0.4)	1,393.7	(1)
1,361.5	(0.4)	1,361.5	(0.4)	1,361.0	(0.5)
1,313.1	(0.5)	1,312.8	(0.2)	1,312.5	(1)
1,287.7	(0.4)	1,288.1	(0.2)	1,287.5	(0.5)
1,225.0	(0.4)	1,226.6	(0.4)	1,226.4	(0.5)
1,205.0	(0.3)	1,205.3	(0.3)	1,205.2	(0.3)
1,153.4	(0.5)	1,153.9	(0.3)	1,153.5	(1)
1,067.7	(0.3)	1,068.1	(0.3)	1,067.6	(0.5)
1,018.8	(0.3)	1,019.0	(0.2)	1,018.6	(0.5)
861.3	(0.4)	861.7	(0.3)	861.3	(0.5)
830.6	(0.5)	831.4	(0.3)	830.4	(0.5)
730.3	(0.3)	730.7	(0.3)	730.4	(0.5)
592.2	(0.3)	592.3	(0.4)	591.9	(1)
534.1	(0.3)	534.4	(0.4)	533.8	(0.5)
381.7	(0.4)	381.8	(0.3)	381.3	(0.3)
203.9	(0.4)	203.8	(0.3)	203.5	(1)

Note: Errors (3σ) are given in brackets.

6 | CONCLUSION

We have performed wavenumber and intensity calibration of a Raman spectrometer using pure rotational ($\Delta\nu = 0, \Delta J = \pm 2$) Raman bands of H_2, HD, D_2, and vibration–rotation bands ($\Delta\nu = 1, \Delta J = \pm 2$) of O_2. Accurate theoretical transition wavenumbers for molecular hydrogen (including its isotopologues) and experimental results from high-resolution Raman spectroscopy of O_2 have been used for the wavenumber calibration. Relative experimental intensities for bands originating from common rotational states and the corresponding accurate theoretical ratios were used with a nonlinear fitting procedure to obtain the wavelength-dependent sensitivity for intensity calibration. Polarization dependence has been corrected by comparing the observed depolarization ratio, ρ, for the pure rotational Raman bands (H_2, HD, and D_2) and vibration–rotation bands (O_2), with the theoretical value of $\rho = 0.75$.

Wavenumber and intensity calibration were performed for the broad Raman spectral range covering −1,036 to 1,700 cm^{-1} (502–583 nm or 17,150–19,900 cm^{-1} in absolute wavenumbers). This spectral region is available for measurement using the second harmonic of Nd:YAG as well as argon ion lasers, thus enabling measurement of calibrated Raman spectra falling within −1,036 to 1,700 cm^{-1} using 532-nm excitation, ~600–3,330 cm^{-1} using 488-nm excitation, and ~1,950–4,685 cm^{-1} using 457.9-nm excitation. Previously reported results on theoretical wavelength-dependent polarizability anisotropy[24,58] for H_2, HD, and D_2 enable intensity calibration procedure reported here to be applied also to other wavelength excitations.

Data set on the relative Raman intensities of carbon tetrachloride, cyclohexane, benzene, toluene, and benzonitrile (in Table 3) reported here serves as a reference for direct intensity calibration using Raman intensities of these common organic liquids. This enables a simple and straightforward intensity calibration scheme applicable for a wide variety of Raman spectrometers. In addition, this approach for intensity calibration using organic liquids is fast, convenient, and fairly accurate (with errors <5%) and covers both Stokes and anti-Stokes regions as well the two polarizations. Vibrational frequencies of indene are updated (Table 4), which serves as a reference for routine wavenumber calibration.

Application of Raman spectroscopy for quantitative analysis requires knowledge of absolute Raman cross-sections. The experimental determination of absolute Raman cross-sections is possible by comparison of Raman intensities of the target molecule with a reference. This needs accurate intensity calibration of the Raman spectra because the involved vibrational bands of target and reference usually have different transition wavenumbers. Accurate intensity calibration discussed here enables such experimental determination of absolute Raman cross-sections.

Theoretical models toward vibrational transition wavenumbers and Raman intensities involve approximations such as employing harmonic potential for obtaining the Hessian while keeping terms up to the second order in the Taylor series expansion, using only the first-order geometrical derivative of the polarizability invariants, and more. Experimental vibrational transition wavenumbers and relative Raman intensities reported here for select organic liquids provide standards for comparison with results from theoretical techniques,[59,60] albeit limited to the liquid phase.

Intensity calibration using the outlined approach of employing pairs of pure rotation and rotation–vibration bands has scope for improvements. The availability of accurate wavelength-dependent matrix elements of polarizability for O_2 allows for reducing the accuracy of this present calibration beyond 1,450 cm^{-1}. N_2 is another candidate molecule for similar calibration in the high wavenumber region around 2,330 cm^{-1} using rotation–vibration Raman bands as shown here using

O_2. However, the calculation of high accuracy wavelength-dependent polarizabilities as obtained for H_2 and isotopologues is difficult for O_2 and N_2 due to high computational costs.

Wavenumber and intensity calibration procedures for Raman spectrometers presented here provide accurate calibration essential for accurate spectroscopic measurements, such as temperature determination from Raman spectra, measurement of standardized Raman spectra, determination of Raman cross-sections, and overall a vital step toward the standardization of Raman spectroscopy.

ACKNOWLEDGEMENTS

This work was supported by the Ministry of Science and Technology, Taiwan (Grants MOST105-2923-M-009-001-MY3, MOST108-2113-M-009-010-MY3, and MOST103-2113-M-009-001) and the Center for Emergent Functional Matter Science of National Chiao Tung University from the Featured Areas Research Center Program within the framework of the Higher Education Sprout Project by the Ministry of Education (MOE), Taiwan. Authors thank Prof. T. Ishibashi and Dr. M. Okuno (from University of Tsukuba, Japan) for helping with the design of the gas cell.

SUPPLEMENTARY MATERIAL AND DATA AVAILABILITY

Supplementary Material (26 pages) includes the following content. Section 1: Details on correction for obtaining spectra as photons/wavenumber; Section 2: Concept of the fitting scheme for intensity calibration; Section 3: Error analysis of band area from rotational Raman bands; Section 4: Transitions wavenumbers and vibration–rotation correction factors for O_2 for J=3–45; Section 5: Error analysis for wavenumber calibration; Section 6: Correction curves for intensity calibration obtained from the fit; Section 7: Results for perpendicular polarization (wavenumber calibration, broadband white light spectra, wavelength-dependent sensitivity using rotational and vibration rotation bands, and temperature determination from water); Section 8: Fitting results for pure rotation bands for O_2 for intensity calibration; Section 9: Standard spectra of organic liquids (carbon tetrachloride, cyclohexane, benzene, toluene, and benzonitrile); and Section 10: Raman spectra of indene with marked band positions and respective uncertainties. Programs written in Igor Pro[35] and Python[36] for wavenumber and intensity calibrations are available on GitHub[27] indexed with the DOI: 10.5281/zenodo.3364647.

ORCID

Ankit Raj https://orcid.org/0000-0002-2495-3354
Henryk A. Witek https://orcid.org/0000-0002-9013-1287
Hiro-o Hamaguchi https://orcid.org/0000-0002-4320-0921

REFERENCES

[1] J. Loader, *Basic Laser Raman Spectroscopy*, Heyden and Sons Ltd., London **1970**.
[2] D. Strommen, K. Nakamoto, *Laboratory Raman Spectroscopy*, Wiley, New York **1984**.
[3] H. Hamaguchi, *Appl Spectrosc Rev* **1988**, *24*, 137.
[4] R. L. McCreery, in *Modern Techniques in Raman Spectroscopy*, (Ed: J. J. Laserna), John Wiley & Sons, New York **1996**, 41.
[5] R. L. McCreery, *Raman Spectroscopy for Chemical Analysis*, John Wiley & Sons, New York **2000**.
[6] S. B. Kim, R. M. Hammaker, W. G. Fateley, *Appl. Spectrosc.* **1986**, *40*, 412.
[7] A. Kramida, Yu. Ralchenko, J. Reader, and NIST ASD Team, NIST Atomic Spectra Database (ver. 5.6.1), [Online]. Available: https://physics.nist.gov/asd [2019, May 20]. National Institute of Standards and Technology, Gaithersburg, MD. **2018**.
[8] N. C. Craig, I. W. Levin, *Appl. Spectrosc.* **1979**, *33*, 475.
[9] ASTM E1840–96(2014), *Standard Guide for Raman Shift Standards for Spectrometer Calibration*, ASTM International, West Conshohocken, PA **2014**.
[10] I. Langmuir, *Phys. Ther. Rev.* **1916**, *7*, 302.
[11] R. Stair, W. E. Schneider, J. K. Jackson, *Appl. Optics* **1963**, *2*, 1151.
[12] D. P. Verret, K. G. Ramanathan, *J. Opt. Soc. Am.* **1978**, *68*, 1167.
[13] S. Montero, D. Bermejo, M. A. Lopez, *Appl. Spectrosc.* **1976**, *30*, 628.
[14] J. W. McConkey, J. M. Woolsey, *Appl. Optics* **1969**, *8*, 205.
[15] K. Iwata, H. Hamaguchi, M. Tasumi, *Appl. Spectrosc.* **1988**, *42*, 12.
[16] M. Fryling, C. J. Frank, R. L. McCreery, *Appl. Spectrosc.* **1993**, *47*, 1965.
[17] K. G. Ray, R. L. McCreery, *Appl. Spectrosc.* **1997**, *51*, 108.
[18] H. Hamaguchi, I. Harada, T. Shimanouchi, *Chem Lett* **1974**, *3*, 1405.
[19] H. Okajima, H. Hamaguchi, *J Raman Spectrosc* **2015**, *46*, 1140.
[20] M. Schlösser, S. Rupp, H. Seitz, S. Fischer, B. Bornschein, T. M. James, H. H. Telle, *J. Mol. Struct.* **2013**, *1044*, 61.
[21] J. Komasa, K. Piszczatowski, G. Łach, M. Przybytek, B. Jeziorski, K. Pachucki, *J Chem Theory Comput* **2011**, *7*, 3105.
[22] K. Pachucki, J. Komasa, *Phys. Chem. Chem. Phys.* **2010**, *12*, 9188.
[23] H. G. M. Edwards, D. A. Long, K. A. B. Najm, M. Thomsen, *J Raman Spectrosc* **1981**, *10*, 60.
[24] A. Raj, H. Hamaguchi, H. A. Witek, *J. Chem. Phys.* **2018**, *148*, 104308.
[25] A. Raj, H. A. Witek, H. Hamaguchi, *Mol Phys* **2019**, *2019*, 1632950. https://doi.org/10.1080/00268976
[26] M. A. Buldakov, V. N. Cherepanov, B. V. Korolev, I. I. Matrosov, *J Mol Spectrosc* **2003**, *217*, 1.
[27] A repository containing a Igor procedures and Python modules for wavenumber and intensity calibration using Raman spectra from H_2, HD, D_2 and O_2. https://github.com/ankit7540/RamanSpecCalibration, Accessed: 2020-06-25.
[28] L. Bytautas, N. Matsunaga, K. Ruedenberg, *J. Chem. Phys.* **2010**, *132*, 074307.
[29] B. Valeur, *Molecular Fluorescence: Principles and Applications*, Wiley-VCH, Verlag GmbH, New York **2001**.
[30] G. Angulo, G. Grampp, A. Rosspeintner, *Spectrochim. Acta A* **2006**, *65*, 727.
[31] J. Mooney, P. Kambhampati, *J Phys Chem Lett* **2013**, *4*, 3316.
[32] J. Mooney, P. Kambhampati, *J Phys Chem Lett* **2014**, *5*, 3497.

[33] D. A. Long, *The Raman Effect: A Unified Treatment of the Theory of Raman Scattering by Molecules*, John Wiley & Sons Ltd., Chichester, England **2002**.
[34] C. M. Penney, R. L. S. Peters, M. Lapp, *J. Opt. Soc. Am.* **1974**, *64*, 712.
[35] Igor Pro, WaveMetrics, Lake Oswego, OR, USA, version 7, A scientific data analysis software with numerical computing environment and a programming language.
[36] G. Rossum, Python reference manual, CWI (Centre for Mathematics and Computer Science), Amsterdam, The Netherlands, **1995**; T. E. Oliphant, *Guide to NumPy*, Trelgol Publishing, USA, **2006**; E. Jones, T. Oliphant, P. Peterson et al., SciPy: Open source scientific tools for Python, Accessed: 2019-09-02, 2001–.
[37] P. T. Boggs, R. H. Byrd, R. B. Schnabel, *SIAM J Sci Comput* **1987**, *8*, 1052.
[38] P. T. Boggs, J. R. Donaldson, R. H. Byrd, R. B. Schnabel, *ACM Trans Math Softw* **1989**, *15*, 348.
[39] J. W. Zwolak, P. T. Boggs, L. T. Watson, *ACM Trans Math Softw* **2007**, *33*, 27.
[40] R. Keijser, J. Lombardi, K. V. den Hout, B. Sanctuary, H. Knaap, *Phys. Ther.* **1974**, *76*, 585.
[41] M. P. L. Flohic, P. Duggan, P. M. Sinclair, J. R. Drummond, A. D. May, *Can J Phys* **1994**, *72*, 186.
[42] T. Shimanouchi, *Nat Stand Ref Data Ser, Nat Bur Stand* **1967**, *6*, 1.
[43] G. E. Walrafen, *J. Chem. Phys.* **1964**, *40*, 3249.
[44] W. Kiefer, J. A. Topp, *Appl. Spectrosc.* **1974**, *28*, 26.
[45] G. Chantry, *Spectrochim. Acta A* **1965**, *21*, 1007.
[46] K. Fukushi, M. Kimura, *J Raman Spectrosc* **1979**, *8*, 125.
[47] Y. Saito, T. Ishibashi, H. Hamaguchi, *J Raman Spectrosc* **2000**, *31*, 725.
[48] J. M. Fernández-Sánchez, S. Montero, *J. Chem. Phys.* **1989**, *90*, 2909.
[49] M. Tasumi, T. Urano, M. Nakata, *J. Mol. Struct.* **1986**, *146*, 383.
[50] C. G. Hickman, J. R. Gascooke, W. D. Lawrance, *J. Chem. Phys.* **1996**, *104*, 4887.
[51] J. Green, D. Harrison, *Spectrochim Acta, Part a* **1976**, *32*, 1279.
[52] A. G. Császár, G. Fogarasi, *Spectrochim Acta, Part a* **1989**, *45*, 845.
[53] I. Harada, J. Hiraishi, *Laser Raman Spectroscopy and Its Applications*, Nanko-do, Tokyo **1976**.
[54] W. K. Bischel, D. J. Bamford, L. E. Jusinski, *Appl. Optics* **1986**, *25*, 1215.
[55] V. Sivaprakasam, D. K. Killinger, *J Opt Soc Am B* **2003**, *20*, 1980.
[56] T. Yamauchi, I. Yanagisawa, *Appl. Optics* **1985**, *24*, 700.
[57] F. Flora, L. Giudicotti, *Appl. Optics* **1987**, *26*, 4001.
[58] A repository containing a FORTRAN program, a Python module along with polarizability data and rovibrational wavefunctions, for the calculation of rovibrational matrix elements of polarizability for H_2, HD and D_2. https://github.com/ankit7540/H2PolarizabilityMatrixElements, Accessed: 2020-06-25.
[59] G. Placzek, *Handbuch der Radiologie*, Vol. 2, Akademische Verlagsgesselschaft VI, Leipzig **1934**, 209.
[60] E. B. Wilson Jr., J. C. Decius, P. C. Cross, *Molecular Vibrations: The Theory of Infrared and Raman Vibrational Spectra*, Dover Publications, New York **1955**.

SUPPORTING INFORMATION

Additional supporting information may be found online in the Supporting Information section at the end of this article.

How to cite this article: Raj A, Kato C, Witek HA, Hamaguchi H. Toward standardization of Raman spectroscopy: Accurate wavenumber and intensity calibration using rotational Raman spectra of H_2, HD, D_2, and vibration–rotation spectrum of O_2. *J Raman Spectrosc*. 2020;1–17. https://doi.org/10.1002/jrs.5955